Faraday Discussions

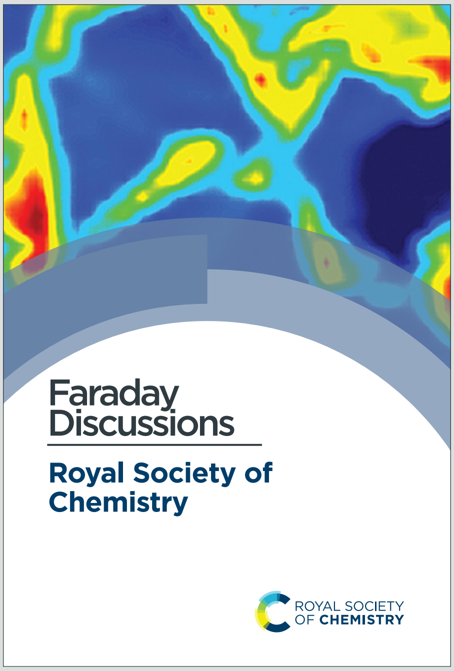

This article can be cited before page numbers have been issued, to do this please use: A. S. Metlay, S. Park, S. C. Bracco and L. E. Marbella, *Faraday Discuss.*, 2026, DOI: 10.1039/D6FD00051G.

www.rsc.org/faraday_d

View Article Online
DOI: 10.1039/D6FD00051G

Decoupling interfacial processes in the formulation of fluorine-free lithium metal batteries

Amy S. Metlay,[1] Susie Park,[1] Sophia C. Bracco,[2] Lauren E. Marbella[1,]*

[1]Department of Chemical Engineering, Columbia University, New York, NY 10027, USA

[2]Department of Chemistry, Barnard College, Columbia University, New York, New York 10027, USA

Abstract

Fluorine additives in lithium metal batteries are often correlated with improved performance, yet lead to challenges associated with cost, health, and safety. In this work, we formulate a series of electrolytes that allow us to interrogate the physical and electrochemical properties of non-fluorinated and fluorinated anions (nitrate, bis(oxalato)borate, and hexafluorophosphate) on the reversible electrodeposition of Li metal via traditional surface characterization methods, spectroscopy, and electroanalytical techniques. When the salts are used in the moderate concentration regime (0.5 M Li), the solid electrolyte interphases (SEIs) generated during cycling are primarily solvent-derived and are statistically similar in terms of ionic transport properties. Nuclear magnetic resonance (NMR) in conjunction with transient voltammetry measurements indicate that Li metal CE is correlated with charge transfer, which is strongly influenced by Li^+ solvation structure. Specifically, we find that the nitrate anion displaces solvent molecules in the Li^+ solvation sphere, leading to tunable solvation/desolvation dynamics. We demonstrate that these metrics can be utilized to construct fluorine-free electrolytes containing lithium nitrate and lithium bis(oxalato)borate for high performance lithium metal anodes.

Introduction

Modern electrolyte design for Li metal batteries (LMBs) requires controlling Li^+ solvation structure to improve Coulombic efficiency (CE).[1-3] Successful efforts to tune the solvation sphere around Li^+ rely heavily on fluorinated salts and solvents (e.g., high concentrations of lithium bis(fluorosulfonyl)imide (LiFSI), lithium bis(trifluoromethanesulfonyl)imide (LiTFSI), fluoroethylene carbonate (FEC), fluorinated ether diluents),[4-8] leading to a long-standing correlation between the properties imparted by fluorine in both the liquid electrolyte and the solid electrolyte interphase (SEI) on CE. For example, weakly coordinating solvents often contain fluorine atoms (e.g., FEC and fluorinated ethers, especially in combination with LiFSI) that do not strongly coordinate to Li^+ thus increasing the concentration of contact-ion pairs

View Article Online
DOI: 10.1039/D6FD00051G

(CIPs) and aggregates (AGGs) in solution compared to solvent-separated ion pairs (SSIPs).[3,9-11] These species shift the equilibrium potential of Li/Li^+ upward, minimizing electrolyte decomposition, thinning the SEI, and improving CE.[12,13] Likewise, altering the solvation structure within the electrolyte changes the chemical species that are delivered to the surface of Li metal during electrochemical cycling, allowing for chemical- and spatial-tuning of SEI structures.[14] Ultimately, this allows the CIPs and AGGs to enrich the SEI with inorganic phases within the "inner" portion of the SEI (i.e., closest to the electrode),[15,16] leading to a strong correlation between the amount of LiF in the SEI and CE.

However, the use of fluorinated electrolyte components (e.g., LiFSI, LiTFSI, fluorinated ethers) presents several issues, including cost,[17] toxicity,[18] and thermal instability.[19] For example, differential scanning calorimetry (DSC) measurements show that the thermal decomposition of LiFSI releases about twice as much heat as lithium hexafluorophosphate ($LiPF_6$), presenting serious safety risks. In addition, many of these compounds and their degradation products are perfluoroalkyl substances (PFAS), (i.e., compounds that contain at least one perfluorinated carbon),[20] that are hazardous to the environment and human health. Further, their specific role and necessity for overall LMB performance has recently been called into question.[21-23] The correlation between LiF in the SEI and high CE is counterintuitive because LiF is a poor Li^+ conductor (bulk conductivity = 10^{-14} S/cm),[24] suggesting that other features may be responsible for improved performance. For instance, recent work from Hobold and coworkers found a stronger positive correlation between Li_2O vs LiF content in the SEI and CE, which is a more ionically conductive phase.[22] Further, additional spectroscopic work suggests that in high performance LMBs the LiF phase in the SEI undergoes structural changes (e.g., nanosizing, compositional doping).[25,26] These structural alterations result in superior interphasial transport properties, indicating that morphology and non-fluorinated chemistries may also benefit Li cyclability. Taken together, these data indicate that alternative low- to no-fluorine electrolyte systems may achieve similarly high cycling efficiencies for Li without the associated cost, health, and safety challenges.[27-29]

In this work, we formulate a series of fluorinated and non-fluorinated electrolytes to examine the role that non-fluorinated anions play in determining Li metal CE. We perform these experiments in the moderate concentration regime (0.5 M Li salt), which improves the cost- and density-related shortcomings of more concentrated electrolytes while still allowing us to tune Li^+ solvation environment. We use $LiPF_6$ to benchmark our systems and compare to various mixtures of lithium bis(oxalato)borate (LiBOB) and lithium nitrate ($LiNO_3$), which offer the ability to passivate Al and achieve high ionic conductivity in the SEI, respectively.[30-32] Through a combination of nuclear magnetic resonance (NMR), electrochemistry, and surface analysis we find that the role of solvation and subsequent stripping/plating dynamics in moderately concentrated electrolytes dominates CE performance over SEI composition. Specifically, we find that the addition of NO_3^- in electrolytes expedites the rate of lithium stripping, but that NO_3^- alone results in poor plating, likely due to strong solvation sphere interactions. Thus, a balance in

View Article Online
DOI: 10.1039/D6FD00051G

solvation strength that properly weighs both solvation and desolvation needs must be met. We leverage this balance to formulate high CE (~97.8 ± 0.2%) fluorine-free Li||Cu half cells for LMB applications.

Results

Electrolyte formulations

We first prepared six electrolyte formulations that contain different molar ratios of 0.5 M (total salt concentration) LiBOB, $LiPF_6$, and $LiNO_3$ in 1:1 (vol%) of ethylene carbonate (EC):1,2-dimethoxyethane (DME) (Figure 1). Herein, single salt formulations will be referred to based on their anion identity, e.g., LiBOB/$LiPF_6$ combinations will be referred to as PB, LiBOB/$LiNO_3$ combinations will be referred to as BN, and $LiPF_6$/$LiNO_3$ combinations will be referred to as PN. Number ratios preceding a combination nomenclature correspond to the relative ratio of each salt (e.g., 1:4 BN represents a 1:4 LiBOB:$LiNO_3$ electrolyte).

At 0.5 M total Li salt concentration in EC:DME, we avoid solubility limitations associated with these salts, allowing us to systematically tune the Li^+ solvation environment. Due to the large donor number[33] associated with the anion, $LiNO_3$ displays poor solubilities in standard carbonate-based electrolytes, requiring ether-based solvents like DME for ion dissociation.[34] Beyond solubility constraints, DME displays low dielectric capabilities due to low polarity. Accordingly, we incorporate EC into our solvent mixture for to its high dielectric constant (ε ~90)[35] and enabling high ionic conductivity.

View Article Online
DOI: 10.1039/D6FD00051G

For our salts, we targeted mixed systems that we anticipated would exhibit different solvation environments about Li^+. Following Lewis basicity trends, we expect PF_6^- to weakly coordinate to the Li^+ cation, favoring a solvent-rich Li^+ inner solvation sphere. In contrast, NO_3^- is a strong Lewis base, and even at 0.5 M, may displace solvent molecules surrounding Li^+ to form contact-ion pairs that alter SEI compositions and Li plating behavior.[36] BOB^- represents a midpoint in anion Lewis basicity, and may disrupt solvent and NO_3^- interactions in multicomponent systems. We theorize two possible outcomes for resultant SEI composition from this electrolyte series. Firstly, SEIs constructed from BOB^--based decomposition products are known to have high structural stability but low ionic conductivity,[30,32] while conversely NO_3^--based decomposition products are known to have comparatively high ionic conductivity.[34] Thus, BN compositions may result in structurally robust and highly ionically conductive SEIs, favorable characteristics for LMB performance. Alternatively, due to the moderate concentration of our electrolytes, we expect solvent molecule coordination to dominate the Li^+ solvation shell, consequently leading to dominant solvent decomposition and thus a primarily organic SEI regardless of specific electrolyte formulation.

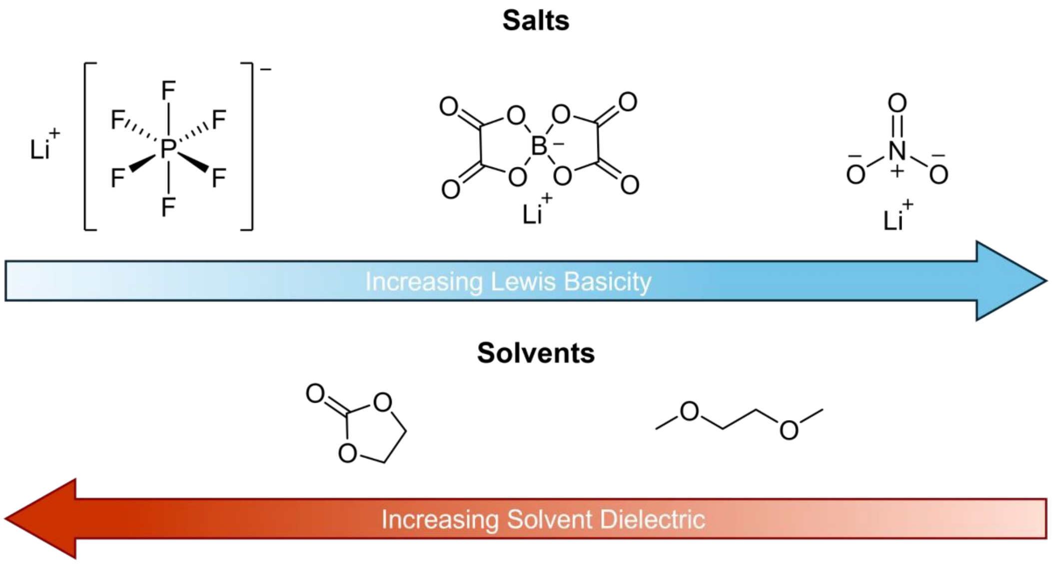

Figure 1. Molecular structures of the salts and solvents used in this study. Salts and solvents are listed according to increasing Lewis Basicity from left to right. Solvents are listed according to increasing dielectric constants from right to left.

Using ^7Li and ^{17}O Liquid-State NMR to Characterize Li^+ Solvation Environment

To probe Li^+ solvation structure, we conduct a series of ^7Li and ^{17}O NMR experiments that measure the local structure around the Li-ion and the solvent molecules. Figure 2a shows the ^7Li NMR spectra of 0.5 M $LiPF_6$, LiBOB, $LiNO_3$, 1:1 PB, 1:1 PN, and 1:1 BN. When these salts dissolve in EC:DME, electron donors on the solvent molecules (e.g., oxygen atoms from carbonyl and ether groups) interact with Li^+. Upon coordination, the Li^+ environment is populated with more electron density, resulting in a chemical shift towards values lower than 0 ppm for all solvated Li^+ species. We see the most negative shift for the $LiPF_6$ electrolyte at -1.45 ppm, indicating that the Li^+ cation environment is highly shielded with electron density from electron donating solvent molecules, and likely spends most of its time solvent-separated from the PF_6^- anion. The presence of solvent-separated Li^+ cations is further supported by analysis of the ^{17}O NMR spectrum of 0.5 M $LiPF_6$ (Fig. 2b, S3, Table S2). In ^{17}O NMR, peaks represent a population-weighted average of the oxygen groups from free solvent and the oxygen atoms coordinated to Li^+ due to rapid exchange between those two environments.[37] The magnitude of the chemical shift compared to that of the neat solvent (here, EC:DME) is related to the population difference between free and coordinated solvent molecules. In the case of the $LiPF_6$ electrolyte solvent, we see the largest negative shift for the EC carbonyl (Δ = -3.3 ppm, Table S2) and the next largest for the DME ether (Δ = -1.2 ppm, Table S2), suggesting more coordination of Li^+ to the EC carbonyl than the DME ether.

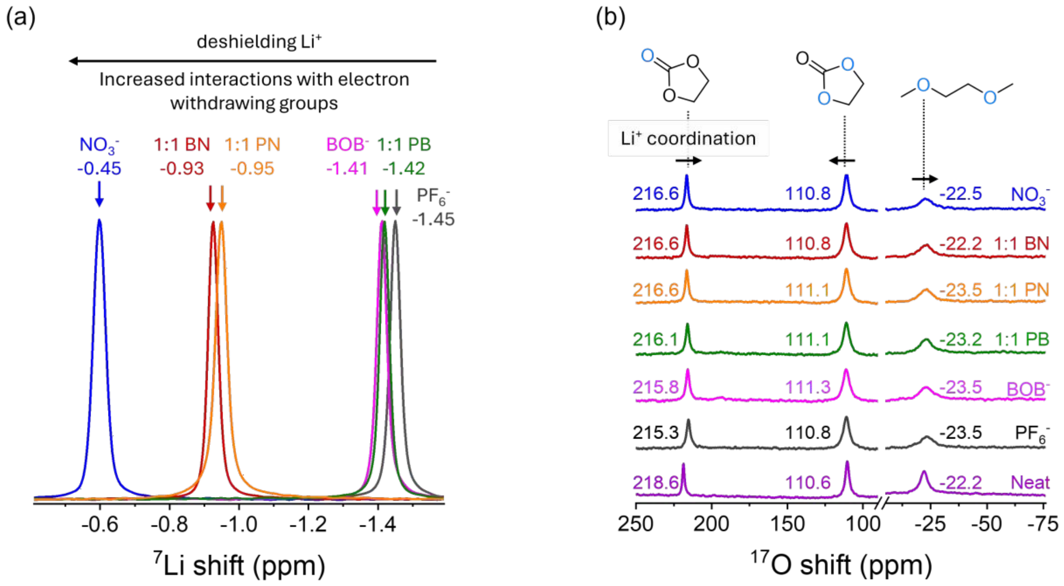

Figure 2. NMR spectra of (a) ^7Li NMR experiments of the solvated Li^+ peak with normalized intensities. Peaks shifted towards higher frequencies (more positive ppm values) indicate deshielding of the solvated Li^+ environment due to interactions with the anions. (b) ^{17}O NMR of EC and DME peaks as specified by blue highlighting in the molecular structure.

We see similar trends in ^7Li NMR and ^{17}O NMR for pure LiBOB and 1:1 PB electrolytes with large negative shifts to lower frequency upon solvation, which suggests that solvents are

DOI: 10.1039/D6FD00051G

coordinating to the Li^+ ions. Compared to the pure $LiPF_6^-$ electrolyte, pure LiBOB and 1:1 PB electrolytes show slightly more positive shifts in ^7Li NMR and slightly more positive EC carbonyl shifts in ^{17}O NMR, suggesting that the BOB^- anion may displace some small molecules in the Li^+ solvation sphere. This change in peak shift magnitude upon addition of the BOB^- anion is less than 1 ppm in reference to the pure $LiPF_6^-$ electrolyte for the ^7Li NMR spectra. A minor change in chemical shift compared to the spectrum of the PF_6^- anion indicates that while more BOB^- interacts with Li^+, the solvation sphere is still primarily solvent dominated.

Upon addition of the NO_3^- anion (pure $LiNO_3$, 1:1 BN, and 1:1 PN), we see comparatively large deshielding towards higher frequency for the Li^+ peak in ^7Li NMR and the primary coordinating solvent oxygen peaks in ^{17}O NMR. This deshielding effect is strongest in pure $LiNO_3$ with a ^7Li shift of +1 ppm when compared to that of $LiPF_6$, and an EC carbonyl shift of +1.3 ppm (again, when compared to the EC carbonyl resonance in ^{17}O NMR for the $LiPF_6$ electrolyte). In ^7Li NMR, both 1:1 PN and 1:1 BN display slightly more modest shifts of +0.5 ppm and +0.7 ppm, respectively, with a similar value of +1.3 ppm for the EC carbonyl peak in ^{17}O NMR. These results suggest that the NO_3^- anion is displacing solvent molecules about the Li^+ cation at a larger fraction than any other probed anion. This interpretation is also supported by an analysis of the full-width at half maximum (fwhm) of the ^{17}O NMR data (see Supplemental Note 1). Thus, even at low salt concentration values of 0.5 M, the NO_3^- displays strong coordination and primary solvation sphere occupation with Li^+.

View Article Online
DOI: 10.1039/D6FD00051G

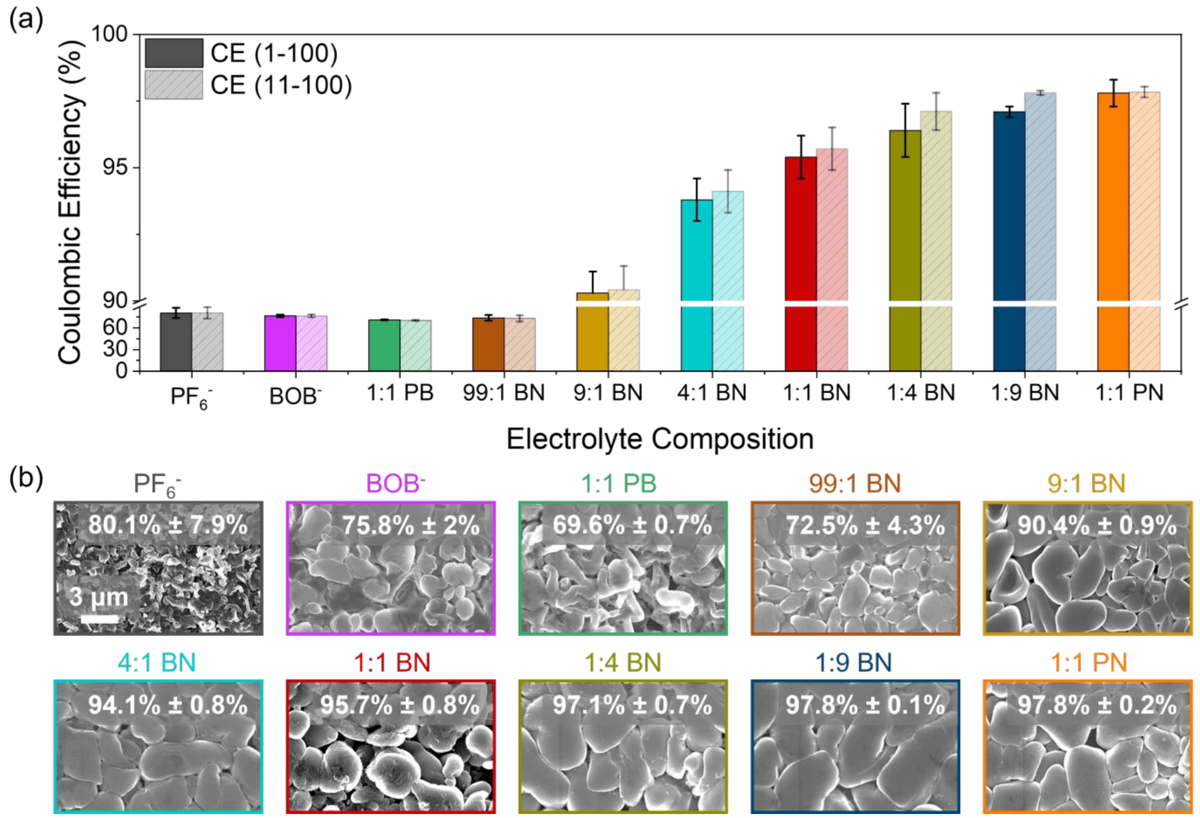

Figure 3. (a) CE results after 100 charge/discharge cycles of Li||Cu half cells run at a 1 hour ± 0.5 mA/cm^2 bias. Left bars represent an average of CE from cycles 1 to 100 over triplicate cells and right bars represent an average of CE from cycles 11 to 100 over triplicate cells. Standard deviation between replicate experiments is shown as an error bar. (b) SEM images of plated lithium on copper current collectors after 4 mAh/cm^2 plating capacity. The top row of SEM images left to right are from PF_6^-, BOB^-, 1:1 PB, 99:1 BN, and 9:1 BN cells. The bottom row of SEM images left to right are from 4:1 BN, 1:1 BN, 1:4 BN, 1:9 BN, and 1:1 PN cells. Values written in the top right corner of the images are CE from cycles 11 to 100.

Evaluating Li cyclability and deposition morphologies

To probe the impact this solvation trend has on LMB performance and surface chemistry, we evaluate Li metal CE in Li||Cu cells, examine the resulting plating morphology with SEM, and characterize the SEI with X-ray photoelectron spectroscopy (XPS). For electrochemical testing and morphological evaluation, we expand to ten different electrolyte formulations, including five additional BN formulations of ratiometrically increasing NO_3^- content. Data for average CE values for Li||Cu cells over the course of 100 cycles are shown in Figures 3a, Figures S5-S15, and Table S5. We find that cells that incorporate little to no NO_3^- (e.g., those with only PF_6^-, BOB^-, 1:1 PB, and 99:1 BN) exhibit lower CE values of 80.1% ± 7.9%, 75.8% ± 2%, 69.6% ± 0.7%, and 72.5% ± 4.3%, respectively, when averaged across cycles 11-100 (Figure 3a). When we increase the relative ratio of NO_3^- while holding total salt concentration the same, we

View Article Online
DOI: 10.1039/D6FD00051G

consistently see an improvement in CE, with the 1:9 BN formulation reaching one of the highest average CE values of 97.8% ± 0.08% for cycles 11-100. This value is similar to the performance of 1:1 PN where the average CE across cycles 11-100 is also equal to 97.8% ± 0.2%. While we attempted to collect CE data on a cell containing only $LiNO_3$ salt in the electrolyte, we repeatedly saw test-ending short circuiting at around the half-way mark of the 100-cycle measurement (Fig. S15).

SEM images of the ten different electrolytes taken after 4 mAh/cm^2 plating capacity show differences in lithium plating morphologies (Figs. 3b, S16, S17). All BN formulations and 1:1 PN show well-packed boulder-like deposits. These boulders appear to grow in size as CE increases, with the high CE 1:1 BN and 1:1 PN morphologies showing large boulders of > 3 μm lateral size while the lower CE 99:1 BN morphology shows smaller boulders of < 3 μm lateral size. Pure LiBOB and 1:1 PB show markedly less uniform growths, with regions of high shape irregularity. The pure $LiPF_6$ electrolyte shows the most dramatic morphological differences from the rest of the electrolyte series displaying granular filaments with plated regions of < 1 μm in lateral size. While large boulder-like morphology can be indicative of high CE in these formulations, plated lithium deposits alone cannot be used as a definitive predictor for cell performance. For example, both 99:1 BN and 9:1 BN cell types show boulder-like plating at < 3 μm lateral size but display vastly different average CE at 72.5% ± 4.3% and 90.4% ± 0.9% from cycles 11-100, respectively.

With a suite of electrolyte formulations that exhibit different electrochemical behavior, we next investigate (i) the impact on SEI compositions and (ii) charge-transfer kinetics to understand their correlation with reversible Li deposition.

Using XPS to compare SEI compositions emerging from different solvation environments

XPS analysis of the residual SEI remaining on Cu after 20 stripping/plating cycles shows that the SEI for all electrolyte formulations is dominated by solvent decomposition products (Table S6 shows that carbon and oxygen make up more than 50% of the total atomic composition). Based on our low salt concentration (0.5 M) and the predominance of SSIPs seen in NMR, we expect solvent molecules, particularly EC, to electrochemically decompose over salt anions like NO_3^-, PF_6^-, and BOB^- during cycling. Even in the case of NO_3^- where the Li^+ solvation sphere contains fewer organic molecules than the other electrolytes, the high concentration of free solvent molecules over solvated inorganic anions still results in a solvent-derived SEI.

From the high resolution C 1s scans we see the presence of C-C, C-O, C=O, and Li_2CO_3 bonding environments at 285 eV, 287 eV, 288 eV, and 290 eV, respectively (Fig. S18, Table S7). In the 1:1 PN cell (CE 97.8%), the compositional breakdown falls between 5-8% for all four carbon environments. Conversely, for the other high performing cell, 1:1 BN (CE 95.7%), the Li_2CO_3 environment dominates at 25%. Further, although nitrogen is an added component in the 1:1 BN

View Article Online
DOI: 10.1039/D6FD00051G

and 1:1 PN cells, the high resolution N 1s scan reveals similarly low nitrogen percent composition for all cells (Fig. S19, Table S8). Analysis of the high resolution O 1s data shows that for both 1:1 BN and 1:1 PN cells, the C=O bonding environment at 532 eV is the highest oxygen component at 32.6% and 15.3% total composition, respectively. However, the C=O environment is also the dominating oxygen component for the low CE BOB$^-$ cell (CE 75.8%) at 25.1%, and a large percentage of the low CE 1:1 PB cell (CE 69.6%) at 22.0% (Fig. S20, Table S9). Additional compositional features such as boron and phosphorus are not present in both high-performance cells (e.g., 1:1 PN shows phosphorus but no major boron environments, while 1:1 BN shows no major phosphorus but some boron environments), so we cannot point to any obvious overlap between high CE from high resolution XPS (Fig S21, S22, Table S10, S11). As expected, high resolution F 1s reveals that the BOB$^-$, NO_3^-, and 1:1 BN cells do not contain any fluorine, confirming that cross-contamination does not play a role in the observed electrochemical properties (Fig. S24, Table S13).[38]

We statistically rate the relationship between SEI atomic compositions for different electrolyte formulations and CE via a cosine similarity analysis. In this test, a calculated value of 1 indicates perfect similarity, and a calculated value of 0 indicates no similarity (Fig. S25, see Supporting Information for further discussion on the statistical method). We find that two high CE cells, 1:1 PN and 1:1 BN at 97.8% and 95.7%, have a low cosine similarity score of approximately 0.55, indicating low similarity for SEI composition. Additionally, two low CE performing cells, 1:1 PB and PF_6^- at 69.9% and 80.1% CEs, show a low cosine similarity score of approximately 0.65. These low similarity scores indicate low correlation between performance and total SEI composition. In fact, a relatively high cosine similarity score of approximately 0.85 is found between 1:1 BN and 1:1 PB, two cells displaying opposite performances. Overall, these data indicate that there is minimal statistical correlation between the primarily solvent-based SEI atomic composition and CE for these electrolytes. Instead, we suspect that decreased solvent content in the solvation shell (where systems with less EC in the Li^+ solvation sphere, such as 1:1 PN show higher CE than cells with higher EC solvation content such as 1:1 PB) impacts charge-transfer processes at the interfaces that may be mechanistically probed via electroanalytical methods.

Measuring exchange current density in the presence of an SEI

First, we measure stationary potentiostatic electrochemical impedance spectroscopy (PEIS), one of the most utilized electrochemical protocols in Li battery literature,[39-41] in the presence of a native SEI (we denote these measurements nPEIS). We collect nPEIS measurements at 5-hour intervals immediately after cell assembly over the course of a 65 hour rest period (Fig. S27). In general, all cells display an increase in resistance over time that we ascribe to native SEI formation and wetting (Fig. S28). Following the low-overpotential Butler-Volmer approximation,[42] this resistance increase corresponds to a decrease in exchange current density,

View Article Online
DOI: 10.1039/D6FD00051G

j_0, as the SEI develops in all of the cells, indicating that the transport of Li^+ ions through the SEI decreases with SEI growth (Fig. S28, Table S14). We find that across all time points, the 1:1 PN cell displays the largest value of j_0 with the 1:1 PB cell showing the next highest values of j_0 after the first measurement point. As 1:1 PN and 1:1 PB cells display opposite performance values, we do not see a clear trend between either the rate of SEI growth nor j_0 in the presence of a native SEI at any of the time points and CE (Figs. S28).

Next, we measure PEIS following electrochemical deposition of Li (denoted ePEIS) to understand how transport of Li^+ through the SEI generated after formation impacts j_0. We take ePEIS measurements every 10 minutes during the first 1 mA/cm^2 charging period with a 1-minute rest inserted between the 10-minute 1 mA/cm^2 bias and the stationary PEIS measurement. For each ePEIS experiment, we take a total of six PEIS scans, resulting in an overall charging capacity of 1 mAh/cm^2 at the conclusion of the experiment (see Fig. S29 for experimental schematics and Fig. S30 for example Nyquist plots). All cell types display a decrease in measured resistance and thus an increase in j_0 as a function of charge capacity (Fig. S31, Table S14). This decrease in resistance is most pronounced for poorly performing cells (e.g., the cell containing NO_3^- that short circuited, and the pure-component cells) and least pronounced for cells cycled with 1:1 PB and 1:1 PN electrolytes that exhibit CE values >95%, possibly indicating that the electrochemically SEI stabilizes quickly in high performing cells (Fig. S31b). Increasing values of j_0 across the measurements may suggest that the transport of Li^+ ions through the electrochemically-derived SEI becomes easier with continued cycling. Alternatively, as we take ePEIS measurements after plating steps, the active surface area of the lithium at each measurement point may be changing according to the nonuniform deposition morphologies identified in Fig. 3. As such, the slight increase in j_0 values may be due to increasing active surface area. Still, we note that the j_0 values derived from ePEIS do not show substantial deviation between individual electrolyte formulations. For example, cells with opposing performance such as 1:1 PB and 1:1 BN show similar values of $j_0 = 0.7 \pm 0.04$ mA/cm^2 and 0.6 ± 0.07 mA/cm^2, respectively at the 30 min measurement point, but have CE values of 69.9% and 97.8%. In other words, transport through the electrochemically formed SEI does not seem to be a largely variable factor in this electrolyte series.

Measuring exchange current density in the absence of an SEI

Next, we perform cyclic voltammetry (CV) measurements on tungsten ultramicroelectrodes (UMEs) at transient scan rates of 10 V/s (Fig. S33) to eliminate the presence of Li^+ transport through the SEI and isolate charge transfer kinetics dominated by solvation/desolvation events. When we use rapid scan rates, the interface does not have time to form an SEI during an individual voltammetry sweep (unlike our EIS measurements). These measurements allow us to extract the j_0 that corresponds to electron transfer by analyzing the low overpotential region of the stripping portion of the voltammogram (Fig. 4a).[39,43]

View Article Online
DOI: 10.1039/D6FD00051G

During analysis, we normalize j_0 for each electrolyte type from individual electrodes to the results obtained from PF_6^- to account for uncontrollable differences in electrochemically active surface area between different electrodes. In Fig. 4b, we see that the addition of NO_3^- to BOB^-- and PF_6^--based electrolytes to make 1:1 BN and 1:1 PN formulations results in a roughly 3-fold increase in j_0 while the 1:1 PB cell displays a normalized j_0 value similar to that of BOB^- and PF_6^- (Fig. 4b, Table S14). This substantial increase in j_0 for 1:1 BN and 1:1 PN cells signifies that the addition of NO_3^- to the electrolyte greatly increases the rate of charge transfer in our mixed electrolyte formulations. Recall that these two formulations also exhibit high Li metal CE (95.7% and 97.8%for 1:1 BN and 1:1 PN, respectively).

While beneficial to the rate in mixed salt systems, the NO_3^- electrolyte on its own does not display a high value of normalized j_0 as derived from the stripping portion of the voltammogram. However, it is important to consider stripping results in the larger context of plating as the stripping reaction is ultimately limited by the amount of lithium that is successfully plated onto the working electrode. Upon analyzing the plating region of the voltammogram, we see that the NO_3^- cell has a significantly smaller normalized plating slope than other NO_3^- containing formulations (Fig. 4c). This small slope indicates that plating from an entirely NO_3^--based electrolyte is challenging. Therefore, in the case of the NO_3^- voltammogram, we have less Li metal plated on the UME that can be stripped during the return wave of the CV experiment, resulting in a correspondingly low value of calculated j_0. This small plating slope is unique to NO_3^-, and thus the availability of plated lithium to strip is not a major limitation for the other

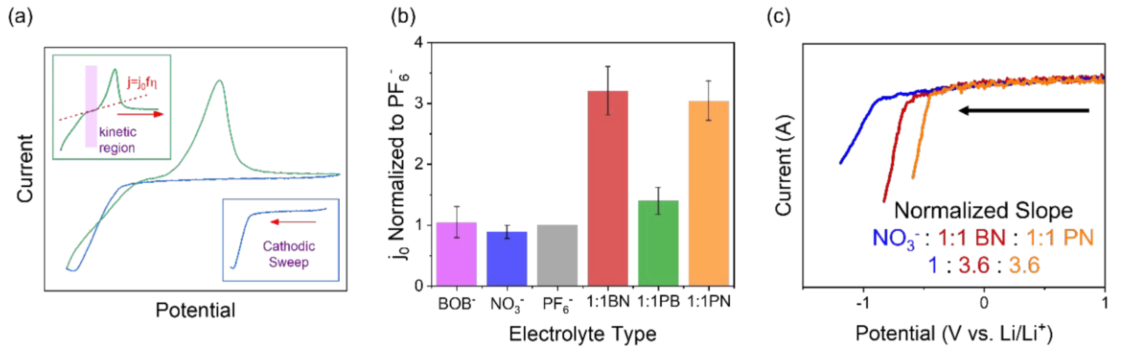

Figure 4. (a) Schematic of the analysis conducted on transient CV scans. The green portion of the CV represents the anodic stripping sweep of the experiment. The pink highlighted region in the upper left inset marks the low-overpotential kinetic region of the voltammogram. Values of j_0 are extracted from the slope of a linear fit conducted in this region. (b) Chart displaying the j_0 values calculated from the stripping portion of transient CV experiments. The j_0 value calculated for each electrolyte type for each individual electrode is normalized to the j_0 value calculated for the PF_6^- electrolyte to account for small area differences between multiple different ultramicroelectrodes (UMEs). Results represent the average from at least three electrode scans with error bars displaying the standard deviation between replicate experiments. (c) Plating slope from transient CV experiments. Reported CV plots are not IR corrected,[39] and do not show substantial changes upon an IR correction.

View Article Online
DOI: 10.1039/D6FD00051G

electrolyte formulations (Fig. S33). The larger plating slopes of 1:1 PN and 1:1 BN systems imply that adding an additional anion to a NO_3^--containing system results in more facile plating.

The NO_3^- anion is a strongly coordinating high donor-number salt and, as shown in our NMR results, dominates the solvation shell of Li^+ over solvent coordination, meaning that Li^+ solvation is stronger in NO_3^- containing electrolytes. This conclusion is consistent with previous literature, which suggests that when solvation of a Li^+ cation is exceptionally strong, dendritic growth dominates, increasing the risk of short circuiting as is seen in the pure $LiNO_3^-$ cell (Fig. S15).[43]

Discussion

Our data indicates that solvation shell dynamics, specifically the ability for the Li^+ cation to solvate and desolvate in a facile fashion, is a significant factor in CE performance for moderately concentrated, fluorine-free LMB electrolytes. We find that coordination strength of the solvation shell, and thus rate of the stripping/plating reaction, can be tuned with NO_3^- concentration (Fig. 5a). When ion-ion interactions are too strong, even in relatively diluted electrolytes, as is the case with the 100% NO_3^- system as indicated by the small CV plating slope, Li^+ desolvation has a large barrier and plating is unfavorable. Analysis of ^7Li and ^{17}O chemical shifts and linewidths support that such a solvation sphere is composed of fewer solvent molecules compared to anion

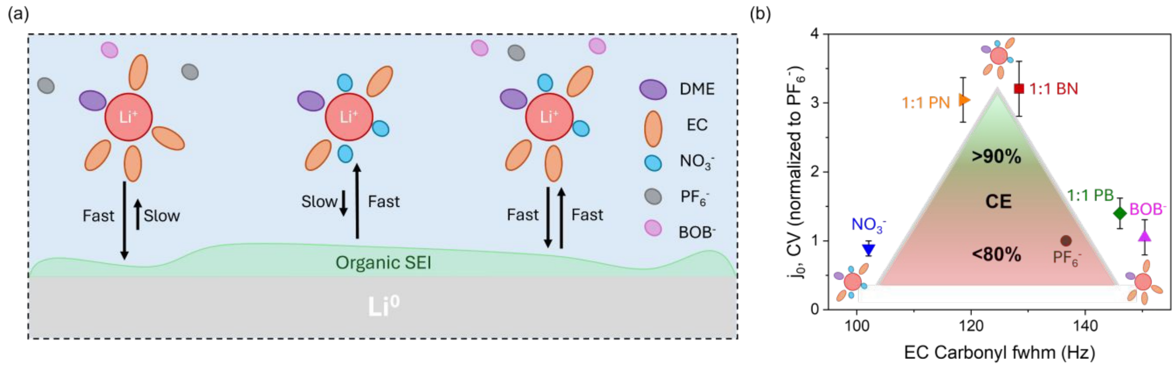

Figure 5. (a) Cartoon describing the changing solvation and desolvation dynamics that occur based on solvation sphere composition. When no NO_3^- is included in the electrolyte (and thus the solvation sphere is solvent dominated) the desolvation of the Li^+ cation is fast, but solvation is slow. This is represented by the leftmost solvation shell. When too much NO_3^- is included in the electrolyte (and thus the solvation sphere has less solvent) the desolvation of the Li^+ cation is slow, but solvation is fast. This is represented by the middle solvation shell. Finally, when an ideal balance of NO_3^- in the electrolyte (and thus the solvation sphere) is reached, both desolvation and solvation are fast. (b) Volcano relationship between desolvation strength (represented as j_0 extracted from the stripping portion of the transient CV experiment) and EC carbonyl fwhm. Values near the top of the volcano (e.g. 1:1 PN and 1:1 BN) exhibit high CE, and values near the bottom of the volcano (e.g. NO_3^-, 1:1 PB, BOB^-, and PF_6^-) exhibit low CE or consistent cycle ending shorting.

View Article Online
DOI: 10.1039/D6FD00051G

pairs that are weaker Lewis bases (like BOB$^-$ or PF_6^-). When solvation is too weak, as is the case for electrolytes with no NO_3^- anions, such as 1:1 PB, BOB$^-$, and PF_6^- as indicated by the low j_0 value calculated from CV experiments, solvation of Li^+ upon stripping is not a strong driving force and Li metal CE suffers. ^{7}Li and ^{17}O NMR indicate that the Li^+ cations are increasingly coordinated by solvent molecules in these formulations. Thus, we use these datasets to construct a volcano-shaped plot to illustrate the balance between strength of solvation/desolvation and its relationship to Li^+-solvent interactions from ^{17}O NMR that these electrolytes must meet to achieve high CE for Li, as is the case for our 1:1 BN and 1:1 PN formulations (Fig. 5b).

The correlation between CE and Li^+ solvation dynamics rather than ionic transport through the SEI is likely impacted by the fact that all formulations evaluated in this work lead to solvent-derived passivation layers. No cell type displays a composition made of uniquely conductive SEI constituents. Instead, XPS shows that all SEIs exhibit high concentrations of phases like C=O (likely from EC reduction), an environment not expected to show any uniquely facile ionic conductivity. As such, the transport of the Li^+ cation as probed by EIS techniques is similarly hindered in all cell types, and the solvation dynamics measured via transient voltammetry emerges as the unique determinant between cells.

From these above results, we can rationalize a few directives for the formulation of fluorine-free electrolytes for LMBs, particularly in the moderate salt concentration regime. Specifically, the influence of fluorine-derived phases in the SEI does not appear to dominate or play a significant role in determining Li metal CE. Therefore, adding fluorinated salts solely for the purpose of tailoring the SEI is ineffective at moderate concentrations and does not improve the CE of cells. Instead, adding a salt with a strongly coordinating anion such as $LiNO_3$ should be utilized to tune the Li^+ solvation sphere and improve the solvation and subsequent stripping kinetics of the reaction.

Conclusion

Beyond the formulation of fluorine-free electrolytes for LMBs, this work highlights the importance of optimizing electrochemical methodology for a specific battery chemistry. While stationary PEIS is a prevalent electrochemical technique in literature, it very specifically probes ionic transport through the SEI, and can readily become subject to overfitting and over analysis if attempts are made to separate out specific components. Furthermore, ionic transport through the SEI is not necessarily the performance determinant process in every battery chemistry and thus PEIS is not always the ideal electrochemical technique for all investigations. Rather, for chemistries displaying similar SEIs across an electrolyte series, as is the case in this work, transient voltammetry coupled with solvation-probing spectroscopy to investigate solvation dynamics may be more appropriate, whereas ePEIS describes the rate of passivation. Following this logic, a similar stepwise investigation of different electrochemical techniques for higher concentration fluorine-free LMB electrolytes may reveal a different ideal electrolyte formulation

View Article Online
DOI: 10.1039/D6FD00051G

than that proposed here and would help to further our understanding of the role of specific electrolyte components on performance.

Author Contributions

A.S.M and L.E.M conceptualized the study. A.S.M. carried out all experimental investigation and formal analysis. S.P. aided in data acquisition and formal analysis of XPS results. S.C.B. aided in the data acquisition of voltammetry results. A.S.M. and L.E.M. wrote the manuscript, which was reviewed and edited by all authors.

Conflicts of interest

There are no conflicts to declare.

Data availability

Data for this article, including NMR, XPS, and cycling data are available at The Open Science Framework at https://doi.org/10.17605/OSF.IO/BKQAW.

Acknowledgements

This work was supported by the National Science Foundation (NSF) CAREER Award (CBET-2045262). S.C.B. would like to thank Barnard College and the Office of the Provost for additional support. The authors acknowledge the use of facilities and instrumentation supported by NSF through the Columbia University, Columbia Nano Initiative, and the Materials Research Science and Engineering Center DMR-2011738.

References

1 Qian, J., Henderson, W. A., Xu, W., Bhattacharya, P., Engelhard, M., Borodin, O., Zhang, J. G. High rate and stable cycling of lithium metal anode. *Nature Comm.* **2015**, *6*, 6362. https://doi.org/10.1038/ncomms7362
2 Suo, L., Hu, Y., Li, H., Armand, M., Chen, L. A new class of Solvent-in-Salt electrolyte for high-energy rechargeable metallic lithium batteries. *Nature Comm.* **2013**, *4,* 1481. https://doi.org/10.1038/ncomms2513
3 Dong, L., Zhong, S., Yuan, B., Ji, Y., Liu, J., Liu, Y., Yang, C., Han, J., He, W. Electrolyte Engineering for High-Voltage Lithium Metal Batteries. *Research,* **2022,** *2022,* 9837586. https://doi.org/10.34133/2022/9837586

View Article Online
DOI: 10.1039/D6FD00051G

4 Weber, R., Genovese, M., Louli, A. J., Hames, S., Martin, C., Hill, I. G., Dahn, J. R. Long cycle life and dendrite-free lithium morphology in anode-free lithium pouch cells enabled by a dual-salt liquid electrolyte. *Nat Energy* **2019**, *4*, 683-689. https://doi.org/10.1038/s41560-019-0428-9

5 May, R., Hestenes, J. C., Munich, N. A., Marbella, L. E. Fluorinated ether decomposition in localized high concentration electrolytes. *J. Power Sources* **2023**, *553*, 232299. https://doi.org/10.1016/j.jpowsour.2022.232299

6 Tan, J., Matz, J., Dong, P., Shen, J., Ye, M. A Growing Appreciation for the Role of LiF in the Solid Electrolyte Interphase. *Adv. Energy Mater* **2021**, *11*, 2100046. https://doi.org/10.1002/aenm.202100046

7 Fan, X., Chen, L., Ji, X., Xu, K., Wang, C. *et al.* Highly Fluorinated Interphases Enable High-Voltage Li-Metal Batteries. *Chem*, **2018**, *4*, 174-185. https://doi.org/10.1016/j.chempr.2017.10.017

8 Cao, X. *et al.* Monolithic solid-electrolyte interphases formed in fluorinated orthoformate-based electrolytes minimize Li depletion and pulverization. *Nat. Energy*, **2019**, *4*, 796-805. https://doi.org/10.1038/s41560-019-0464-5

9 Liu, B., Zhang, J., Xu, W. Advancing Lithium Metal Batteries. *Joule* **2018**, *2*, 833-845. https://doi.org/10.1016/j.joule.2018.03.008

10 Wang, J., Ge, B., Li, H., Yang, M., Wang, J., Liu, D., Fernandez, C., Chen, X., Peng, Q. Challenges and progresses of lithium-metal batteries. *Chem. Eng. J.* **2021,** *420, 129739.* https://doi.org/10.1016/j.cej.2021.129739

11 Li, T., Zhang, X., Shi, P., Zhang, Q. Fluorinated Solid-Electrolyte Interphase in High-Voltage Lithium Metal Batteries. *Joule,* **2019**, *3*, 2647-2661. https://doi.org/10.1016/j.joule.2019.09.022

12 Fang, Z., Ko, S., Yamada, A. Manipulating the Potential Diagram for Better Lithium-Metal Batteries. *ACS Energy Lett.* **2025**, *10*, 3526-3532. https://doi.org/10.1021/acsenergylett.5c00832

13 Ko, S., Obukata, T., Shimada, T., Takenaka, N., Nakayama, M., Yamada, A., Yamada, Y. Electrode potential influences the reversibility of lithium-metal anodes. *Nat. Energy* **2022**, *7*, 1217-1224. https://doi.org/10.1038/s41560-022-01144-0

14 Pokharel, J. *et al.* Manipulating the diffusion energy barrier at the lithium metal electrolyte interface for dendrite-free long-life batteries. *Nature Comm.* **2024**, *15*, 3085. https://doi.org/10.1038/s41467-024-47521-z

15 Yu, Z. *et al.* Molecular design for electrolyte solvents enabling energy-dense and long-cycling lithium metal batteries. *Nat. Energy*, **2020**, *5*, 526-533. https://doi.org/10.1038/s41560-020-0634-5

16 Zheng, J., Lochala, J., Kwok, A., Deng, Z., Xiao, J. Research Progress towards Understanding the Unique Interfaces between Concentrated Electrolytes and Electrodes for Energy Storage Applications. *Adv. Sci.* **2017**, *4*, 8. https://doi.org/10.1002/advs.201700032

17 Pan, H., Wang, T., Jiang, Y., Ouyang, J., Chen, L., Wang, Z., Song, C., Chen, N., Yan, Q., Li, X., Wu, S., Wang, T., Li, Y. Revisiting Fluorobenzene as Diluents in Ether-Based Electrolytes for Lithium Metal Batteries. *Nature Comm.* **2025**, *16*, 9831. https://doi.org/10.1038/s41467-025-64784-2

18 Botero, P., Ells, A., Svirinovsky-Arbeli, A., Juelsholt, M. & Marbella, L. E. Counterion Lewis Acidity Determines the Rate of Hexafluorophosphate Hydrolysis in Nonaqueous

View Article Online
DOI: 10.1039/D6FD00051G

Battery Electrolytes. *J. Am. Chem. Soc.* **2025**, *147*, 9159-9174. https://doi.org/10.1021/jacs.4c12469

19 Eshetu, G. G., Grugeon, S., Gachot, G., Mathoron, D., Arman, M., Laruelle, S. LiFSI vs. LiPF6 electrolytes in contact with lithiated graphite: Comparing thermal stabilities and identification of specific SEI-reinforcing additives. *Electrochim. Acta.* **2013**, *102*, 133-141. https://doi.org/10.1016/j.electacta.2013.03.171

20 Sarkar, B., Kumawat, R. L., Ma, R., Wang, K., Mohebi, M., Schatz, G. C., Amanchukwu, C. V. Lithium metal-mediated electrochemical reduction of per- and poly-fluoroalkyl substances. *Nat. Chem.* **2026**, *18*, 509-518. https://doi.org/10.1038/s41557-025-02057-7

21 Kim, M. *et al.* Elucidating the Effects of LiF on Lithium Metal Anodes. *Nano Lett.* **2025**, *25*, 14625-14634. https://doi.org/10.1021/acs.nanolett.5c03437

22 Hobold, G. M., Wang, C., Steinberg, K., Li, Y. & Gallant, B. M. High lithium oxide prevalence in the lithium solid-electrolyte interphase for high Coulombic efficiency. *Nat. Energy* **2024**, *9*, 580-591. https://doi.org/10.1038/s41560-024-01494-x

23 Svirinovsky-Arbeli, A., May, R., Kwon, Y., Juelsholt, M. & Marbella, L. E. Perspective Using NMR spectroscopy to link structure to function at the Li solid electrolyte interphase. *Joule* **2024**, *8,* 1919-1935. https://doi.org/10.1016/j.joule.2024.04.016

24 Yildirim, H., Kinaci, A., Chan, M., Greeley, J. First-Principles Analysis of Defect Thermodynamics and Ion Transport in Inorganic SEI Compounds: LiF and NaF. *ACS Appl. Mater. Interfaces* **2015**, *7*, 18985-18996. https://doi.org/10.1021/acsami.5b02904

25 Liu, X., Li, S., Yuan, C., Zheng, B., *et al.* Probing the heterogeneous nature of LiF in solid-electrolyte interphases. *Nature* **2025**, *646*, 102-107. https://doi.org/10.1038/s41586-025-09498-7

26 Shadike, Z., Lee, H., Borodin, O., Cao, X., Fan, X., Wang, X., Lin, R., Bak, S. M., Ghose, S., Xu, K., Wang, C., Liu, J., Xiao, J., Yang, X. Q., Hu, E. Identification of LiH and nanocrystalline LiF in the solid-electrolyte interphase of lithium metal anodes. *Nat. Nanotechnol.* **2021**, *16*, 549-554. https://doi.org/10.1038/s41565-020-00845-5

27 Karanth, P., Weijers, M., Lavrinenko, A. K., Izelaar, B., Kortlever, R., Ganapathy, S., Wagemaker, M., Mulder, F. M. Designing Fluorine-Free Electrolytes for Lithium Metal Batteries. *J. Am. Chem. Soc.* **2025**, *147*, 50, 46008-46022. https://doi.org/10.1021/jacs.5c12584

28 Jiang, Z., Li, C., Yang, T., Deng, Y., Zou, J., Zhang, Q., Li, Y. Fluorine-Free Lithium Metal Batteries with a Stable LiF-Free Solid Electrolyte Interphase. *Energy Lett.* **2024**, *9*, 1389-1396. https://doi.org/10.1021/acsenergylett.3c02724

29 Hernández, G., Mogensen, R., Younesi, R., Mindemark, J. Fluorine-Free Electrolytes for Lithium and Sodium Batteries. *Batteries & Supercaps* **2022**, *5*, 6. https://doi.org/10.1002/batt.202100373

30 Xu, K., Zhang, S., Lee, U., Allen, J., Jow, T. LiBOB: Is it an alternative salt for lithium ion chemistry? *J. Power Sources* **2005**, *146*, 79-85. https://doi.org/10.1016/j.jpowsour.2005.03.153

31 Vinay, B. Nikodimos, Y., Agnihotri, T., Ahmed, S., Hagos, T. M., Hasan, R., Tamilarasan, E. B., Su, W. N., Hwang, B. J. Fluorine-free electrolytes in batteries: principles, strategies, and advances. *Energy Environ. Sci.* **2025**, *18*, 7826-7372. https://doi.org/10.1039/d4ee04820b

View Article Online
DOI: 10.1039/D6FD00051G

32 Melin, T., Lundström, R., Berg, E. Elucidating the Reduction Mechanism of Lithium Bis(oxalato)borate. *J. Phys. Chem. Lett.* **2024**, *15*, 2537-2541. https://doi.org/10.1021/acs.jpclett.4c00328

33 Zhou, P., Xiang, Y., Liu, K. Understanding and applying the donor number of electrolytes in lithium metal batteries. *Energy Environ. Sci.* **2024**, 17, 8057-8077. https://doi.org/10.1039/d4ee02989e

34 Chen, H., Chen, K., Luo, L., Liu, X., Wang, Z., Zhao, A., Li, H., Ai, X., Fang, Y., Cao, Y.. LiNO3-Based Electrolytes via Electron-Donation Modulation for Sustainable Nonaqueous Lithium Rechargeable Batteries. *Angew. Chem. Int. Ed.* **2024**, *63*, 10. https://doi.org/10.1002/anie.202316966

35 Hall, D., Self, J., Dahn, J. Dielectric Constants for Quantum Chemistry and Li-Ion Batteries: Solvent Blends of Ethylene Carbonate and Ethyl Methyl Carbonate. *J. Phys. Chem. C* **2025**, *119*, 22322-22330. https://doi.org/10.1021/acs.jpcc.5b06022

36 Schmid, M., Xu, J., Lindner, J., Novák, P., Schustert, R. Concentration Effects on the Entropy of Electrochemical Lithium Deposition: Implications for Li+ Solvation. *J. Phys. Chem. B* **2015**, *119,* 13385-13390. https://doi.org/10.1021/acs.jpcb.5b07670

37 Bogle, X., Vazquez, R., Greenbaum, S., Cresce, A., Xu, K. Understanding Li+-Solvent Interaction in Nonaqueous Carbonate Electrolytes with 17O NMR. *J. Phys. Chem. Lett* **2013**, *4*, 1664-1668. https://doi.org/10.1021/jz400661k

38 Park, S., Sadowski, J., Kwon, Y., Metlay, A. S., & Marbella, L. E., Electrolyte Vapor Induced Passivation and Transition Metal Redox on Electrode Active Materials. *J. Phys. Chem. C* **2025**, *129*, 20867-20879. https://doi.org/10.1021/acs.jpcc.5c04057

39 Boyle, D. T., Kong, X., Pei, A., Rudnicki, P. E., Shi, F. Huang, W., Bao, Z., Qin, J., Cui, Y. Transient Voltammetry with Ultramicroelectrodes Reveals the Electron Transfer Kinetics of Lithium Metal Anodes. *ACS Energy Lett.* **2020**, *5*, 701-709. https://doi.org/10.1021/acsenergylett.0c00031

40 Hobold, G., Kim, K., Gallant, B. Beneficial vs. inhibiting passivation by the native lithium solid electrolyte interphase revealed by electrochemical Li+ exchange. *Energy Environ. Sci.* **2023**, *16*, 2247-2261. https://doi.org/10.1039/d2ee04203g

41 Guo, R., Gallant, B. Li_2O Solid Electrolyte Interphase: Probing Transport Properties at the Chemical Potential of Lithium. *Chem. Mater.* **2020**, *32*, 5525-5533. https://doi.org/10.1021/acs.chemmater.0c00333

42 Bard, A. J. & Faulkner, L. R. *Electrochemical Methods Fundamentals and Applications second edition*. **2020**.

43 Boyle, D. T., Kim, S. C., Oyakhire, S. T., Vila, R. A., Huang, Z., Sayavong, P., Qin, J., Bao, Z., Cui, Yi. Correlating Kinetics to Cyclability Reveals Thermodynamic Origin of Lithium Anode Morphology in Liquid Electrolytes. *J. Am. Chem. Soc.* **2022**, *144*, 20717-20725. https://doi.org/10.1021/jacs.2c08182

View Article Online
DOI: 10.1039/D6FD00051G

Decoupling interfacial processes in the formulation of fluorine-free lithium metal batteries

Amy S. Metlay,[1] Susie Park,[1] Sophia C. Bracco,[2] Lauren E. Marbella[1],*

[1]Department of Chemical Engineering, Columbia University, New York, NY 10027, USA

[2]Department of Chemistry, Barnard College, Columbia University, New York, New York 10027, USA

Data availability

Data for this article, including NMR, XPS, and cycling data are available at The Open Science Framework at https://doi.org/10.17605/OSF.IO/BKQAW. Additional data supporting this article have been included as part of the Supplementary Information. Supplementary information: Materials and further experimental details, Figures S1-S32, Tables S1-S14, Supplementary Note 1, depicting experimental setups, additional NMR data, electrochemistry, SEM, XPS, cosine similarity analysis.